Theoretical evaluation of three-dimensional elastic constants of native and regenerated celluloses: role of hydrogen bonds

Kohji Tashiro* and Masamichi Kobayashi
Department of Macromolecular Science, Faculty of Science, Osaka University, Toyonaka, Osaka 560, Japan
(Received 28 April 1990; revised 23 May 1990; accepted 31 May 1990)

Three-dimensional elastic constants were calculated for cellulose crystalline forms I and II (native and regenerated celluloses, respectively). The calculated Young's modulus E_l along the chain axis is 167.5 GPa for form I and 162.1 GPa for form II. The E_l of form II has only a slightly lower value than that for form I. This is consistent with the X-ray data (*c.* 120–140 GPa for form I and *c.* 110 GPa for form II) although the absolute values are large. The E_l was found not to be affected by intermolecular interactions but by intramolecular hydrogen bonds along the chain axis, especially the bond between the hydroxyl side group and the ether oxygen atom of the glucose ring (type a). A calculation neglecting this hydrogen bond gives the largely reduced E_l of *c.* 70 GPa. Anisotropy of the Young's modulus and linear compressibility in the planes perpendicular to the molecular chain axis were also calculated. In the form I crystal, where the hydrogen-bonded sheet planes are stacked together by non-bonded van der Waals interactions, the modulus is large within the sheet plane and small in the direction perpendicular to the sheet: the anisotropy is similar to that reported for the nylon 6 α and γ forms. In form II the modulus is large but the anisotropy is not so remarkable, which is similar to atactic poly(vinyl alcohol) and poly(*m*-phenylene isophthalamide). The same tendency is seen also for the linear compressibility. In parallel with the calculation of the elastic constants, the lattice vibrational frequencies were calculated for forms I and II and compared with the observed infra-red and Raman spectral data so as to confirm whether the force fields used were reasonable.

(Keywords: native cellulose; regenerated cellulose; three-dimensional elastic constants; vibrational frequencies; lattice dynamics; hydrogen bonds)

INTRODUCTION

Cellulose exhibits various types of crystal modifications depending on the sample preparation conditions[1,2]. Among these crystal modifications, the most typical and basic crystalline phases are forms I and II, i.e. the native cellulose and the regenerated cellulose, respectively. One of the characteristic properties of cellulose is its significant role as the structural supporter for cell walls of plants, bacteria, papers, etc. Therefore it is very important to interpret the relationship between structure and mechanical properties of cellulose crystals from the molecular theoretical point of view and to predict their limiting mechanical properties. In a long scientific history of cellulose however, the measurement has been limited only to the Young's modulus along the chain axis using X-ray diffraction[3–5]. On the theoretical side, the highly complicated crystal structures of forms I and II have made it practically impossible to calculate the three-dimensional elastic constants. In a series of papers we developed lattice dynamical equations for calculating the three-dimensional elastic constants of polymer systems with complicated structures by utilizing the symmetry properties of the crystals[6]. These equations were applied to the cases of orthorhombic polyethylene[7], poly(vinyl alcohol)[7], nylon 6 α and γ forms[8], poly(vinylidene fluoride) form I[9] and isotactic polypropylene[10]. In the present paper we report the lattice-dynamically calculated three-dimensional anisotropy of the elastic constants for native and regenerated celluloses.

In the theoretical evaluation of the elastic constants, three-dimensional atomic coordinates data and suitable intra- and intermolecular force field parameters must be used. Therefore we have monitored the appropriateness of the structure and force field used here through comparison of the observed and calculated normal-mode frequencies for crystal forms I and II in the frequency region covering the internal and external vibrational modes. Among the intra- and intermolecular interactions, hydrogen bonds of OH · · · O type are expected to play an important role in determining the anisotropic mechanical properties and lattice vibrational frequencies of the celluloses, on which our discussion will be focused.

STRUCTURE AND FORCE FIELD PARAMETERS

Three-dimensional elastic constants and normal-mode frequencies are calculated on the basis of lattice dynamical equations developed in our previous paper[6]. In this method parameters concerning only one crystallographically asymmetric unit are sufficient to obtain information for the overall crystal.

Crystal structure

Crystal structures of cellulose I and II have not been perfectly determined[11–16]. However, X-ray diffraction

* To whom correspondence should be addressed

0032-3861/91/081516-11

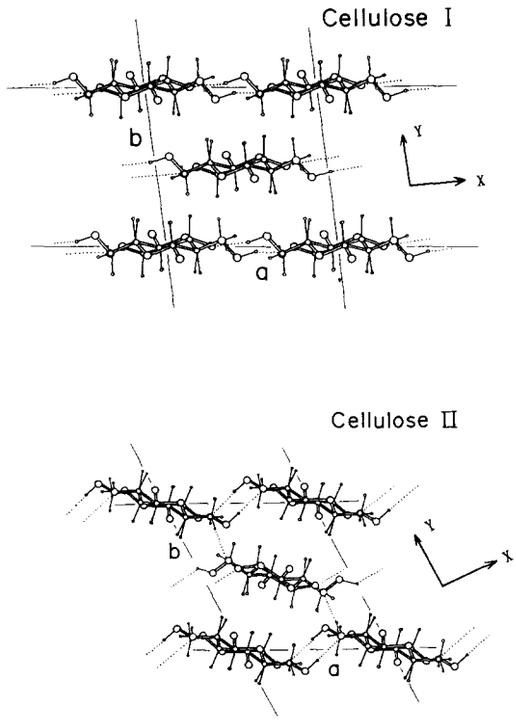

Figure 1 Crystal structures of cellulose forms I and II (projection along the chain axis)[11,13]

data and energy calculations[17–20] basically support the structural models proposed by Blackwell *et al.*[11,13], which are employed in the present calculations. *Figure 1* shows the crystal structures of forms I and II proposed by Blackwell *et al.* The cell constants are as follows: for form I, $a = 8.17$ Å, $b = 7.86$ Å, c(fibre axis) $= 10.38$ Å, $\gamma = 97°$; for form II, $a = 8.01$ Å, $b = 9.04$ Å, c(fibre axis) $= 10.36$ Å, $\gamma = 117.1°$. In *Figure 1* the hydrogen atoms are shown because the intermolecular H · · · H interactions play an important role in determining the anisotropic behaviour of the mechanical constants in the direction perpendicular to the chain axis. The hydrogen atoms were generated so as to satisfy the following geometrical conditions: for the hydrogen atoms in CH_2 and CH groups, the bond length C–H = 1.10 Å and the bond angle $\angle$HOC = 109.5° were assumed; for the hydrogen atoms in OH groups, the bond length O–H = 0.968 Å and the bond angle $\angle$HOC = 109.5° were assumed and the torsional angles around the linkage H–O–C–C were determined in such a way that the hydrogen bond distance O · · · H–O was minimized. This method does not necessarily give the energetically most favourable hydrogen bonds.

The two chains are contained in the unit cell of cellulose I (strictly speaking, the true unit cell contains eight chains and has a cell volume four times larger than that of the basic unit cell shown in *Figure 1*). The molecular chains take an almost fully extended conformation. They are connected with each other by intermolecular hydrogen bonds along the *a* axis to form a sheet-like structure and these sheets are stacked together by van der Waals forces along the *b* axis. In form II, the sheets are connected to each other by hydrogen bonds. The two forms also differ in the packing style of the sheets. In form I all the molecular chains are packed in parallel along the chain axis (the parallel packing structure), while in form II the chains in the adjacent sheets are packed in an anti-parallel mode. Another large difference in structural features between these two forms exists in the intramolecular hydrogen bonds. In form I, as shown in *Figure 2*, intramolecular hydrogen bonds of types *a* and *b* are constructed for both the sides of the chain. In form II the sheets are classified into two types; the sheet at the corner of the unit cell is constructed from chains having both *a* and *b* hydrogen bonds (almost equivalent to the intra-sheet structure of form I) and another sheet at the centre of the unit cell consists only of chains with intramolecular type *a* hydrogen bonds.

Intra- and intermolecular interactions

For the intramolecular interactions a valence force field was employed, and the numerical values of the force constants proposed by Cael *et al.*[21] were used with some modifications: these force constants can reproduce fairly well the infra-red (i.r.) and Raman data in the frequency region 400–3000 cm^{-1}. The force constants f of the O–H · · · O hydrogen bonds were introduced. The values were determined on the basis of the empirical relationship of the f(O–H) and f(O · · · H) *versus* O · · · O distance as proposed by Novak[22], and were modified slightly so as to give the calculated O–H stretching frequencies as close to the observed ones as possible. Appendix I lists the force constants used in the calculation. For the intermolecular force constants the second derivatives of the non-bonded interatomic potentials with respect to the interatomic distance r (in Å) were used, where potential functions of Buckingham and Lennard-Jones type were employed. The f values (in units of mdyn $Å^{-1}$) were given by the following functions: for the H · · · H pairs within 3.2 Å, $f = -7.972/r^8 + 258.01 \exp(-3.74r)$, for the C · · · H pairs within 3.4 Å, $f = -36.5/r^8 + 820.58 \exp(-3.67r)$, and for the O · · · H pairs within 3.0 Å, $f = 2591.41/r^{14}$. For the f values of intermolecular hydrogen bonds the above-mentioned Novak's empirical relation was used (Appendix 1).

Elastic constant tensors

Crystal forms I and II belong to the monoclinic system and the elastic constant tensors are as follows:

$$\boldsymbol{c} = \begin{bmatrix} c_{11} & c_{12} & c_{13} & 0 & 0 & c_{16} \\ c_{21} & c_{22} & c_{23} & 0 & 0 & c_{26} \\ c_{31} & c_{32} & c_{33} & 0 & 0 & c_{36} \\ 0 & 0 & 0 & c_{44} & c_{45} & 0 \\ 0 & 0 & 0 & c_{54} & c_{55} & 0 \\ c_{61} & c_{62} & c_{63} & 0 & 0 & c_{66} \end{bmatrix}$$

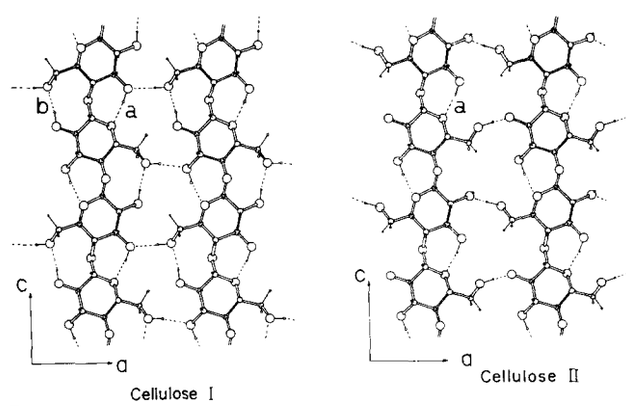

Figure 2 Intramolecular hydrogen bonds in cellulose forms I and II

where the x, y and z axes are defined as shown in *Figure 1* and $xx = 1$, $yy = 2$, $zz = 3$, $yz = 4$, $zx = 5$, and $xy = 6$. For computer calculation, numerical data involving only one glucose-ring residue were prepared. The data on the remaining residues in the unit cell were generated by utilizing the symmetry relation of the crystal (the two-folded screw symmetry and translational symmetry). In the case of form II the chains belonging to the neighbouring sheets are different in the up and down directions along the chain axis and they are symmetrically independent of each other. Therefore the total number of internal coordinates necessary for the calculation of the elastic constants (the bond lengths, bond angles, and internal rotations) reaches *c.* $160 \times 2 = 320$! A calculation based on such a large dimension for the matrices (320×320) is impractical. Two local structures are extracted: (A) the structure surrounding the corner chain of the cells; (B) the structure surrounding the centre chain of the cells. The elastic compliance constants are averaged between models A and B and the constants obtained are used for the real cellulose II crystal.

RESULTS AND DISCUSSION

Appropriateness of the force fields

The calculation for normal modes for cellulose single chains has been reported previously by Cael *et al.*[21] with reasonable results except for the modes associated with hydrogen bonds. In the present calculation the external lattice-mode frequencies were obtained in addition to the intramolecular mode frequencies. The vibrational frequencies calculated for cellulose form I are listed in Appendix 2. In *Figures 3*, *4* and *5* a comparison is made between the calculated frequencies and those actually observed in Raman (4000–300 cm^{-1}) and far-i.r. (400–30 cm^{-1}) spectra of crystal forms I and II, indicating that the calculated results are not so unreasonable when compared with the observed spectra. The degree of vibrational freedom is very large and many bands overlap to result in broad spectra (*Figures 3–5*). Consequently, a detailed comparison of the frequency position of the observed and calculated modes cannot be made directly except for some intense bands. There are several bands which closely relate to the intra- and intermolecular hydrogen bonds[23–25]. We will focus our attention on the vibrational modes of the A symmetry species of cellulose form I. The band at 3412 cm^{-1} (calculated value) is the O–H stretching mode contributed preferentially by the intramolecular hydrogen bond of type *b*, while the 3372 cm^{-1} band is for the hydrogen bond of type *a*. The bands of the O–H stretching modes associated with the intermolecular hydrogen bonds

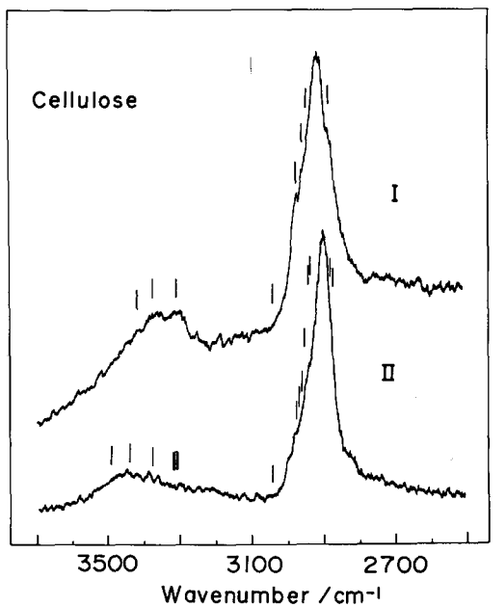

Figure 3 Raman spectra of cellulose forms I (cotton) and II (cellophane) in the region of 2500–3700 cm^{-1}. The vertical bars represent the calculated frequency positions

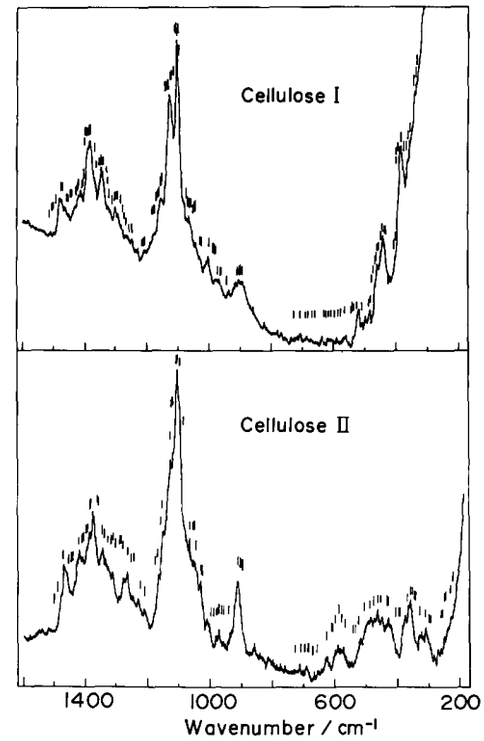

Figure 4 Raman spectra of cellulose forms I (cotton) and II (cellophane) in the region of 200–1600 cm^{-1}. The vertical bars represent the calculated frequency positions

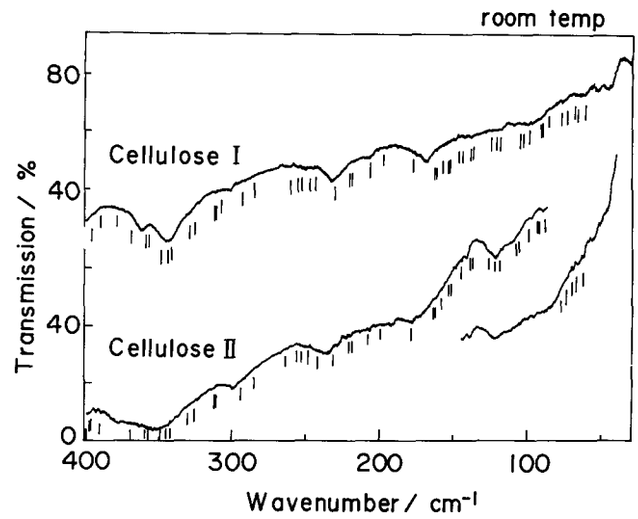

Figure 5 Far-i.r. spectra of cellulose forms I (cotton) and II (cellophane) in the region 30–400 cm^{-1}. The vertical bars represent the calculated frequency positions

appear at lower frequencies around 3300 cm^{-1}. The bond-angle deformation and internal rotation modes related to the hydrogen bonds are calculated to appear in the frequency region below 400 cm^{-1}. For example, in the modes at 430 and 413 cm^{-1} the vibrational potential energy distributes to the bending and torsional coordinates of the intra-chain hydrogen bonds. The bands at 276 and 176 cm^{-1} correspond to the internal rotation modes of the hydrogen-bonded $-CH_2-O-H$ group. The bands at 306, 141 and 117 cm^{-1} are related closely to the O · · · H(O) stretching modes of the intramolecular hydrogen bonds of types *a* (306 and 117 cm^{-1}) and *b* (141 cm^{-1}). As discussed later, these O · · · H(O) internal displacement coordinates, especially of type *a*, contribute significantly to the determination of the magnitude of the Young's modulus along the chain axis. The vibrational modes associated with the hydrogen bonds are in different frequency positions for forms I and II. For example, the O–H stretching modes of the intramolecular hydrogen bonds appear at higher frequency in form II, while those of the intermolecular hydrogen bonds are at almost the same frequency as those for form I. For the O · · · H stretching mode at low frequency the frequencies are higher in form I (see *Table 1*).

This indicates that the intramolecular hydrogen bonds in form II are relatively weaker than those in form I,

Table 1 Vibrational modes associated with hydrogen bonds

	Form I (cm^{-1})	Form II (cm^{-1})
O–H stretching modes		
intramolecular H bonds	3412, 3372	3486, 3315 (model A) 3435, 3374 (model B)
intermolecular H bonds	3309	3309, 3308
O · · · H stretching of type *a*	306, 117	295, 88

while their intermolecular hydrogen bond strength is similar. These differences in hydrogen bond strength reflect a slight difference in the Young's modulus between the two crystal forms, as described below. *Figure 6* shows the lattice vibrational modes of cellulose I. The vibrational frequency of the translational mode along the *b* axis $L(T_b)$ is much higher than those of $L(T_a)$ and $L(T_c)$, suggesting that the shearing modes along the sheet planes occur more easily than the compression mode in the direction perpendicular to the sheet plane. The vibrational modes around the chain axis are predicted to appear at 80 and 54 cm^{-1}, but have not yet been definitely observed in the far-i.r. spectra (*Figure 5*).

Three-dimensional elastic constant matrices

The calculated elastic constant matrices *c* and compliance matrices *s* are:

For form I

$$c = \begin{bmatrix} 54.55 & 1.58 & -2.52 & 0 & 0 & -3.23 \\ 1.58 & 15.16 & 1.26 & 0 & 0 & 4.31 \\ -2.52 & 1.26 & 167.79 & 0 & 0 & 0.51 \\ 0 & 0 & 0 & 3.53 & 1.43 & 0 \\ 0 & 0 & 0 & 1.43 & 8.08 & 0 \\ -3.23 & 4.31 & 0.51 & 0 & 0 & 4.53 \end{bmatrix} \text{GPa}$$

$$s = \begin{bmatrix} 1.99 & -0.84 & 0.03 & 0 & 0 & 2.21 \\ -0.84 & 9.400 & -0.05 & 0 & 0 & -9.53 \\ 0.03 & -0.05 & 0.60 & 0 & 0 & 0.01 \\ 0 & 0 & 0 & 30.53 & -5.42 & 0 \\ 0 & 0 & 0 & -5.42 & 13.35 & 0 \\ 2.21 & -9.53 & 0.01 & 0 & 0 & 32.70 \end{bmatrix} \times 10^{-2}\ \text{GPa}^{-1}$$

For form II

$$c = \begin{bmatrix} 18.07 & 3.84 & 0.60 & 0 & 0 & -0.05 \\ 3.84 & 18.38 & 0.35 & 0 & 0 & 3.72 \\ 0.60 & 0.35 & 162.07 & 0 & 0 & -0.02 \\ 0 & 0 & 0 & 6.08 & -5.03 & 0 \\ 0 & 0 & 0 & -5.03 & 6.29 & 0 \\ -0.05 & 3.72 & -0.02 & 0 & 0 & 5.39 \end{bmatrix} \text{GPa}$$

$$s = \begin{bmatrix} 5.84 & -1.43 & -0.02 & 0 & 0 & 1.04 \\ -1.43 & 6.68 & -0.01 & 0 & 0 & -4.63 \\ -0.02 & -0.01 & 0.62 & 0 & 0 & -0.01 \\ 0 & 0 & 0 & 48.62 & 38.86 & 0 \\ 0 & 0 & 0 & 38.86 & 46.95 & 0 \\ 1.04 & -4.63 & -0.01 & 0 & 0 & 21.77 \end{bmatrix} \times 10^{-2}\ \text{GPa}^{-1}$$

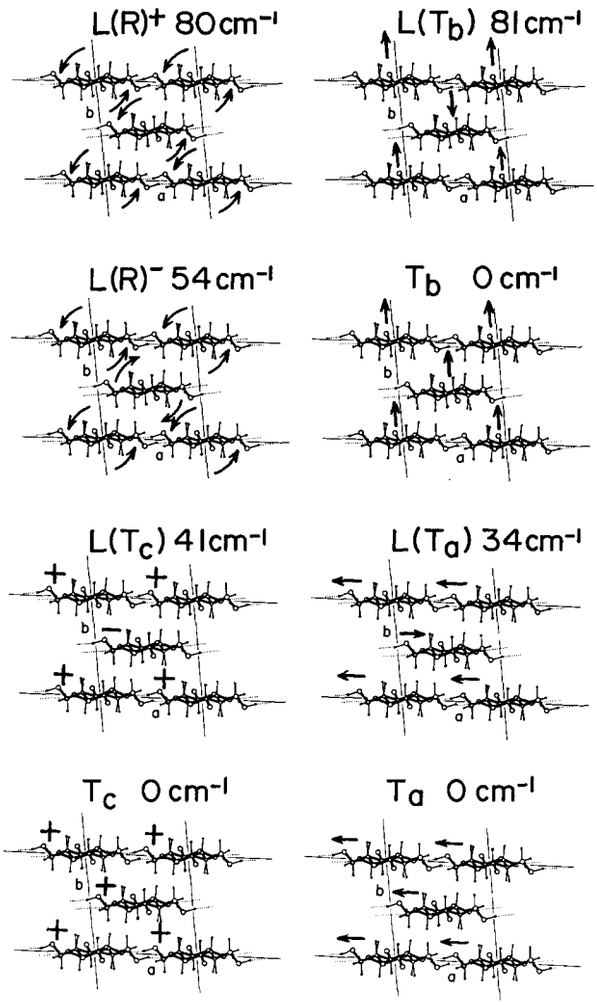

Figure 6 A schematic illustration of the external lattice modes calculated for cellulose form I

Based on these tensors, the Young's modulus along the chain axis E_l and the anisotropy of the Young's modulus and linear compressibility in the planes perpendicular to the chain axis are calculated as follows.

The Young's modulus E_l along the chain axis. The E_l is calculated as $1/s_{33}$. For crystal form I, $E_l = 167.5$ GPa and for form II, $E_l = 162.1$ GPa. The crystallite modulus observed by the X-ray diffraction method under homogeneous tensile stress distribution has been reported as below.

	Sakurada *et al.*[3,4]	Matsuo and Sawatari[5]
Form I	130–138 GPa	120–140 GPa
Form II	90 GPa	106–112 GPa

The observed values are dispersive to some extent, but the difference in E_l between forms I and II is not very large. This corresponds well to the calculated tendency, although the absolute values are much higher in the calculation. A difference in E_l between the theoretical and X-ray observed values is frequently reported. Some of the reasons are as follows.

1. The difference in temperature. The X-ray measurement was carried out at room temperature and the calculation corresponds to the modulus at low temperature where the thermal motion of the chain is frozen. Examples are seen for the cases of orthorhombic polyethylene (PE)[26–28] and trigonal polyoxymethylene (POM)[29–31]. In the case of POM[31], the (true) crystallite modulus at room temperature was estimated as *c.* 75 GPa and that at liquid nitrogen temperature as *c.* 100 GPa. The latter is close to the calculated modulus of 109 GPa, which did not include the effect of thermal motion of the chain.
2. The effect of sample morphology on the observed modulus. The crystallite modulus is usually measured under the assumption that the stress distribution within the sample is homogeneous. Such an assumption is not always suitable and heterogeneous stress distribution must be taken into account in some cases[26,29,31,32]. For POM, for example, the modulus obtained using the homogeneous stress distribution model is 47–73 GPa and is different among the samples employed in the measurements[29–31]. These experimental data were interpreted on the basis of the suitable mechanical model and the true modulus was estimated as *c.* 75 GPa at room temperature after correction for the stress distribution[31].

Figure 7 shows the effects of the various kinds of interactions on E_l, where the moduli are reduced by using the E_l value calculated for cellulose I with all the interactions being taken into account (case A). In the case of form I, E_l is not influenced by intermolecular hydrogen bonds (case B) and intermolecular non-bonded interatomic interactions (case C). In other words, E_l is hardly influenced by intermolecular interactions, as generally reported for other polymer crystals[7–10]. Neglecting the intramolecular hydrogen bond of type *b* also does not affect E_l (case D). However, the modulus is reduced to about 40% of its original value when the type *a* intramolecular hydrogen bond is neglected (case E). *Figure 8* shows the atomic displacements and the strain energy distribution calculated for the cellulose chain subjected to the hypothetically large tensile strain of 10%[33]. The strain energy distributes mainly to the deformation of the glucose rings (*c.* 30%) and the bending of the ether linkages connecting the

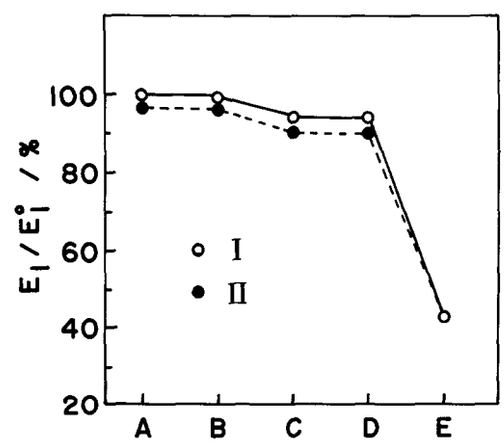

Figure 7 Effects of various types of interactions on the Young's modulus E_l of cellulose forms I (○) and II (●). The modulus is reduced as E_l/E_l^0 where E_l^0 is the Young's modulus of form I crystal calculated with full interactions. (A) With all the interactions taken into account; (B) without including intermolecular hydrogen bonds; (C) neglecting the intermolecular non-bonded interatomic interactions in addition to (B); (D) neglecting the intramolecular hydrogen bonds of type *b* in addition to (C); (E) neglecting the intramolecular hydrogen bonds of type *a* in addition to (D)

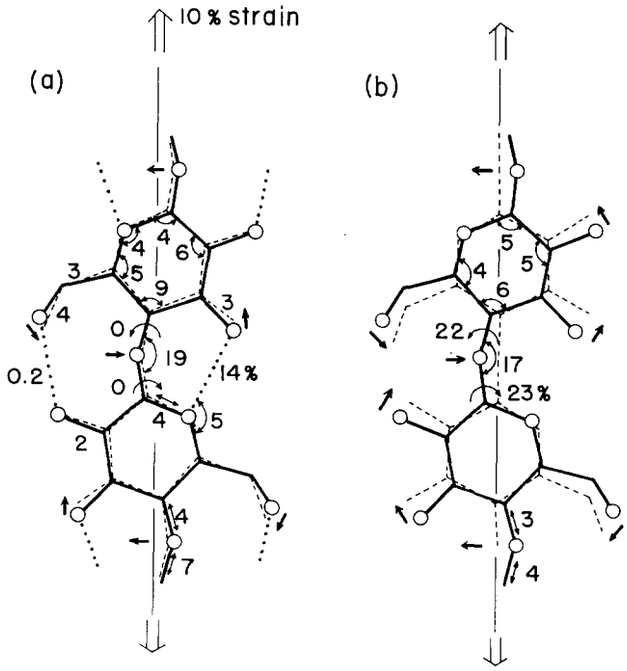

Figure 8 Atomic displacements (internal strains) and strain energy distributions calculated for the mechanically tensioned cellulose chain (a) with and (b) without the intramolecular hydrogen bonds

adjacent rings (*c.* 20%). At the same time the distribution to the type *a* intramolecular hydrogen bond is large, about 20%, while the distribution to the type *b* hydrogen bond is negligibly small. When these intramolecular hydrogen bonds are cut off (by substituting zero values for the corresponding force constants), the strain energy is found to concentrate on the torsional mode around the C–O linkages (45%) and the bending of these bonds (17%), as shown in *Figure 8b*. The cellulose chain is constructed from a linear combination of the glucose rings connected to the C–O single bonds and seems so flexible as to give a low Young's modulus. However, the actual chain gives an unexpectedly high Young's modulus due to the existence of effective intramolecular hydrogen bonds of type *a*. When the chain is in tension along the chain axis, this type of hydrogen bond suppresses the torsional deformation of the flexible ether linkage (as shown in *Figure 8a*) and the mechanical deformation of the chain is due to the bending mode of the skeletal linkages. Hence, the Young's modulus of the cellulose chain is governed by strong intramolecular hydrogen bonds, especially of type *a*.

The same situation is also seen for the case of cellulose form II. As shown in *Figure 2*, one of the structural differences between forms I and II is the presence of type *b* intramolecular hydrogen bonds. But, as discussed above, this type of intramolecular hydrogen bonding has almost no influence upon E_1, indicating that the Young's modulus should not be the same for forms I and II. It is questionable to ascribe the difference in E_l to the existence of type *b* hydrogen bonds as reported by Kroon-Batenburg *et al.*[34]. The difference in E_l is considered to originate from the difference in the strength of the hydrogen bonds. As discussed earlier, the *f* value of the hydrogen bond is slightly smaller in form II than in form I. (This is supported by the difference in the position of the O–H bands in the i.r. and Raman spectra.)

On the basis of the above, we can predict that the Young's modulus of the cellulose chain should be reduced by *c.* 60% if the intramolecular hydrogen bonds are removed. The experimental results reported by Nishino *et al.*[35] support this prediction. They measured the X-ray crystallite modulus of cellulose triacetate (CTA). The fibre period of CTA is about 10.5 Å, close to that of native cellulose (10.4 Å), and is considered to have almost the same skeletal conformation as that of native cellulose[36]. However, CTA has no intramolecular hydrogen bonds because the OH groups are substituted by ester groups. The observed E_l value was only about 33 GPa. Even after the correction for the effective cross-sectional area of the chain (68 Å^2 for CTA and 32 Å^2 for native cellulose), the modulus is only about 50% of that of form I. Strictly speaking, the molecular conformation of CTA may be different from that of the cellulose form I model with the intramolecular hydrogen bonds removed (*Figure 8b*) and therefore the crystallite modulus measured for CTA cannot be compared directly with the theoretical value (*Figure 7*). However, the experimental result for CTA is worth noting in connection with the role of intramolecular hydrogen bonds in determining the Young's modulus of cellulose chains.

In this way the importance of the intramolecular hydrogen bonds in the determination of the Young's modulus E_l of cellulose has been clarified. Such a discussion leads us to the consideration of the Young's modulus of atactic poly(vinyl alcohol) (PVA), for example. We calculated the Young's modulus of syndiotactic PVA to be *c.* 287 GPa[7]. Isotactic PVA possesses strong intramolecular OH · · · O hydrogen bonds along the chain direction[37], leading us to predict that it-PVA exhibits a much higher Young's modulus. In fact the lattice dynamical calculations gives a modulus of about 323 GPa for the it-PVA chain. Therefore we might say that the Young's modulus of at-PVA is enhanced by introducing more isotactic sequences into the skeletal chain.

Mechanical anisotropy in the planes perpendicular to the chain axis. The Young's modulus $E(\theta)$ and the linear compressibility $\beta(\theta)$ in the direction θ from the x axis in the plane perpendicular to the chain axis are calculated using the following equations.

$$1/E(\theta) = s_{11}\cos^4\theta + 2s_{12}\sin^2\theta\cos^2\theta + 2s_{16}\cos^3\theta\sin\theta + s_{22}\sin^4\theta + 2s_{26}\cos\theta\sin^3\theta + s_{66}\cos^2\theta\sin^2\theta$$

$$\beta(\theta) = (s_{11}+s_{12}+s_{13})\cos^2\theta + (s_{21}+s_{22}+s_{23})\sin^2\theta + (s_{16}+s_{26}+s_{36})\sin\theta\cos\theta$$

Figures 9–12 show the anisotropic curves of $E(\theta)$ and $\beta(\theta)$ calculated for celluloses I and II. In these figures the amplitude of the vector from the centre of the cell to a point on the curve represents the magnitude of E or β in this direction. Form I shows an anisotropic curve characteristic of the sheet-like structure similar to that for nylon 6 α and γ forms[8]: the modulus is large in the sheet planes (governed by the hydrogen bonds) and small in the direction perpendicular to it (governed by the van der Waals interactions). In the case of form II, the anisotropy is not so extreme as in form I. This may be due to the effect of the intermolecular hydrogen bonds spreading throughout the unit cells. A similar anisotropy of the modulus is seen also in the cases of PVA[8] and

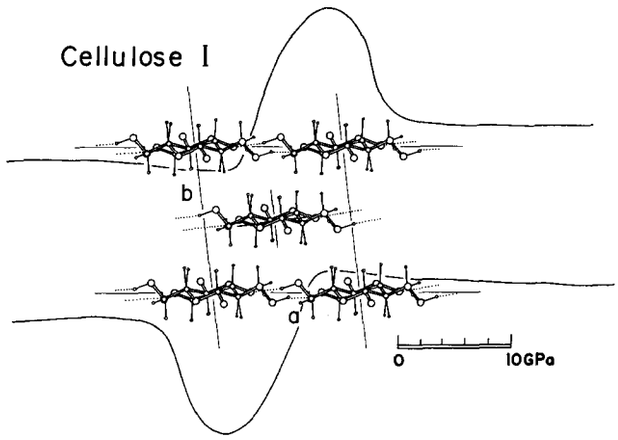

Figure 9 Calculated anisotropic curve of the Young's modulus in the plane perpendicular to the chain axis of cellulose form I

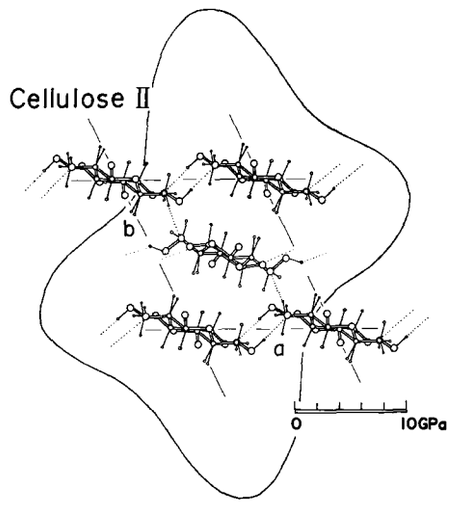

Figure 10 Calculated anisotropic curve of the Young's modulus in the plane perpendicular to the chain axis of cellulose form II

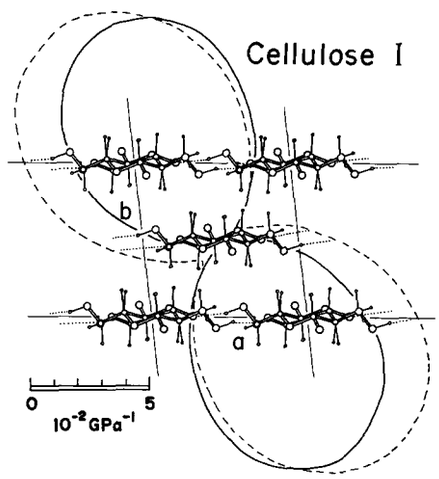

Figure 11 Calculated anisotropic curve of the linear compressibility in the plane perpendicular to the chain axis of cellulose form I. The solid and broken curves are for the calculation with and without the intermolecular hydrogen bonds being taken into account, respectively

poly(*m*-phenylene isophthalamide) (PPIA)[38], where intermolecular hydrogen bonds of the type NH · · · OC are formed in the *a* and *b* directions[39]. *Figure 13* shows the anisotropy of $E(\theta)$ in the planes perpendicular to the chain axis calculated for the PPIA crystal. (The elastic and compliance tensors are listed in Appendix 3.)

Figures 11, *12* and *14* show the role of the intermolecular hydrogen bonds on the anisotropy of the modulus and linear compressibility. Neglecting the intermolecular hydrogen bonds, i.e. using a calculation with only non-bonded interatomic interactions being considered, results in the relatively isotropic curve of the Young's modulus $E(\theta)$. The modulus in the sheet plane of form I is largely reduced by neglecting the intermolecular hydrogen bonds. For form II, the modulus becomes smaller in both the directions of the *a* and *b* axes, though not in the (1 1 0) direction. This behaviour is similar to that for nylon 6 α and γ forms[8]. The effect of hydrogen bonds on the linear compressibility is interpreted in a similar way.

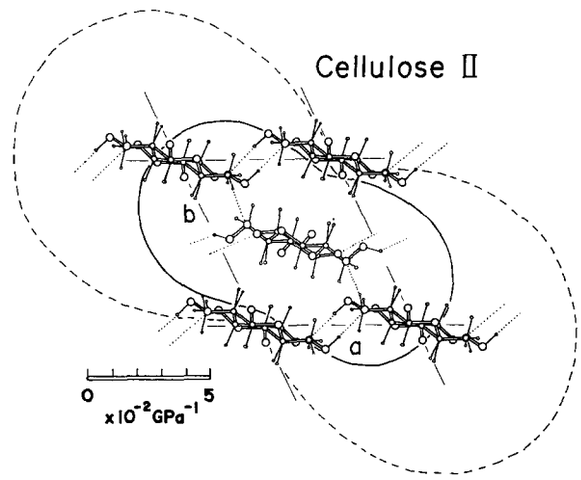

Figure 12 Calculated anisotropic curve of the linear compressibility in the plane perpendicular to the chain axis of cellulose form II. The solid and broken curves are for the calculation with and without the intermolecular hydrogen bonds being taken into account, respectively

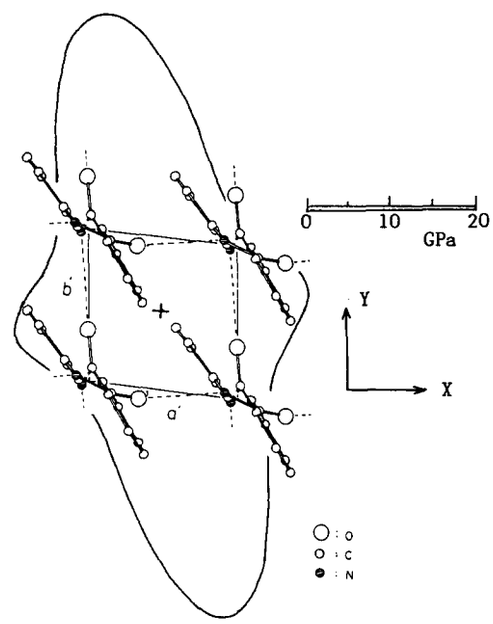

Figure 13 Calculated anisotropic curve of the Young's modulus in the plane perpendicular to the chain axis of poly(*m*-phenylene isophthalamide) crystal

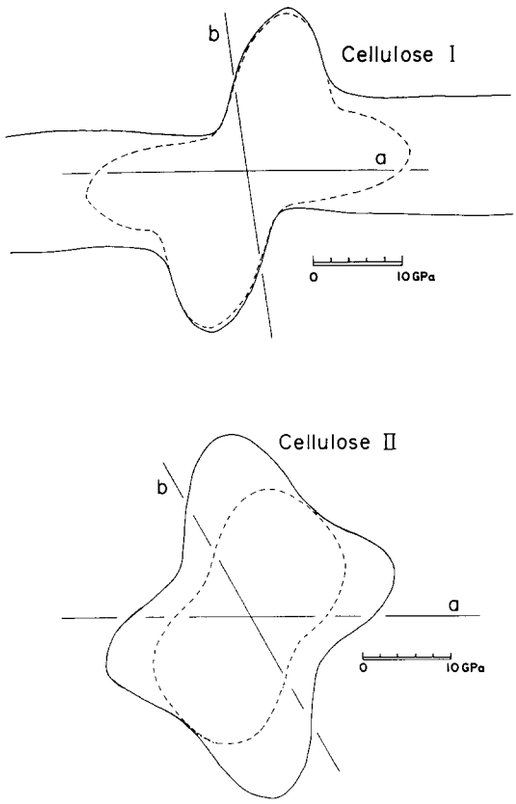

Figure 14 Effect of intermolecular hydrogen bonds on the anisotropic curves of the Young's modulus in the plane perpendicular to the chain axis of cellulose forms I and II: ———, with all the intermolecular interactions; – – –, without the intermolecular hydrogen bonds

CONCLUSIONS

In the present paper we have calculated the three-dimensional elastic and compliance matrices for the cellulose crystal forms I and II on the basis of lattice dynamical treatment. The calculated Young's modulus E_l along the chain axis is 167.5 GPa for form I and 162.1 GPa for form II. The latter has a slightly lower value because of the smaller f value of intramolecular hydrogen bonds of type a, as shown by the higher vibrational frequency of the O–H stretching mode in the i.r. and Raman spectra. The most important factor in determining E_l is the intramolecular hydrogen bonds, especially of type a, and neglecting these bonds reduces the modulus to c. 40%. The E_l is not much affected by the intermolecular non-bonded interactions or the intermolecular hydrogen bonds. An anisotropy of the Young's modulus and linear compressibility in the planes perpendicular to the chain axis were also calculated. The degree of anisotropy is governed by the balance between the intermolecular hydrogen bonds and non-bonded interactions.

Cellulose fibres are basically and practically important in a wide range of fields because of their excellent mechanical properties. In this paper we have clarified an important role of the intra- and intermolecular hydrogen bonds in determining the elastic behaviour of cellulose. It is hoped that the results reported here may act as a guide for developing cellulose fibres with improved mechanical properties.

REFERENCES

1 Young, R. A. and Rowell, R. M. (Eds) 'Cellulose: Structure, Modification and Hydrolysis', Wiley Interscience, New York, 1986
2 Hayashi, J. *Sen-i Gakkaishi (Japan)* 1976, **32**, P-32
3 Sakurada, I., Ito, T. and Nakamae, K. *J. Polym. Sci. C* 1966, **15**, 75
4 Sakurada, I. and Kaji, K. *J. Polym. Sci. C* 1970, **31**, 57
5 Matsuo, M. and Sawatari, C. *Polym. Prepr. Jpn.* 1989, **38**, 980
6 Tashiro, K., Kobayashi, M. and Tadokoro, H. *Macromolecules* 1978, **11**, 904
7 Tashiro, K., Kobayashi, M. and Tadokoro, H. *Macromolecules* 1978, **11**, 914
8 Tashiro, K. and Tadokoro, H. *Macromolecules* 1981, **14**, 781
9 Tashiro, K., Tadokoro, H. and Kobayashi, M. *Ferroelectrics* 1981, **32**, 167
10 Tashiro, K., Kobayashi, M. and Tadokoro, H. *Polym. Prepr. Jpn.* 1986, **35**, 3266
11 Gardner, K. H. and Blackwell, J. *Biopolymers* 1974, **13**, 1975
12 Sarko, A. and Muggli, R. *Macromolecules* 1974, **7**, 486
13 Kolpak, F. J. and Blackwell, J. *Macromolecules* 1976, **9**, 273
14 Stipanovic, A. J. and Sarko, A. *Macromolecules* 1976, **9**, 851
15 Kolpak, I. J., Weih, M. and Blackwell, J. *Polymer* 1978, **19**, 123
16 Matsunaga, H. and Takahashi, Y. *Polym. Prepr. Jpn.* 1987, **36**, 2333
17 Pizzi, A. and Eaton, N. *J. Macromol. Sci. Chem.* 1985, **A22**, 105
18 Pizzi, A. and Eaton, N. *J. Macromol. Sci. Chem.* 1985, **A22**, 139
19 Pizzi, A. and Eaton, N. *J. Macromol. Sci. Chem.* 1987, **A24**, 901
20 Simon, I., Glasser, L., Scheraga, H. A. and St John Manley, R. *Macromolecules* 1988, **21**, 990
21 Cael, J. J., Gardner, K. H., Koenig, J. L. and Blackwell, J. *J. Chem. Phys.* 1975, **62**, 1145
22 Novak, A. *Structure and Bonding* 1974, **18**, 177
23 Liang, C. Y. and Marchessault, R. H. *J. Polym. Sci.* 1959, **37**, 385
24 Liang, C. Y. and Marchessault, R. H. *J. Polym. Sci.* 1959, **39**, 269
25 Marchessault, R. H. and Liang, C. Y. *J. Polym. Sci.* 1960, **43**, 71
26 Clements, J., Jakeways, R. and Ward, I. M. *Polymer* 1978, **19**, 639
27 Barham, P. J. and Keller, A. *J. Polym. Sci., Polym. Lett. Edn* 1979, **17**, 591
28 Nakamae, K., Nishino, T., Ohkubo, H. and Matsumoto, T. *Polym. Prepr. Jpn.* 1987, **36**, 2441
29 Brew, B., Clements, J., Davies, G. R., Jakeways, R. and Ward, I. M. *J. Polym. Sci., Polym. Phys. Edn* 1979, **17**, 351
30 Nakamae, K., Nishino, T., Shimizu, Y., Hata, K. and Matsumoto, T. *Polym. Prepr. Jpn.* 1987, **36**, 2438; *Polymer* in press
31 Tashiro, K., Wu, G. and Kobayashi, M. *Polymer* 1988, **29**, 1768
32 Sawatari, C. and Matsuo, M. *Macromolecules* 1986, **19**, 2726
33 Tashiro, K. and Kobayashi, M. *Polym. Bull.* 1985, **14**, 213
34 Kroon-Batenburg, L. M. J., Kroon, J. and Northolt, M. G. *Polym. Commun.* 1986, **27**, 290
35 Nishino, T., Nakamae, K., Saitaka, K., Azuma, J. and Okamura, K. *Sen-i Gakkai Prepr.* 1989, 1B07
36 Zugenmaier, P. in 'Cellulose: Structure, Modification and Hydrolysis' (Eds R. A. Young and R. M. Rowell), Wiley Interscience, New York, 1986, Ch. 13
37 Tadokoro, H. 'Structure of Crystalline Polymers', Wiley Interscience, New York, 1979
38 Kobayashi, M. and Tashiro, K. *Annual Report of the Research Association for Basic Polymer Technology*, Japan, March 1986
39 Kakida, H., Chatani, Y. and Tadokoro, H. *J. Polym. Sci., Polym. Phys. Edn* 1976, **14**, 427

APPENDIX 1

Table A1 Numerical values of the intramolecular force constants

No.	Coordinates involved	Common atoms	Values[a]
1	C–H (CH_2)		4.626
2	C–H (CH)		4.688
3	C–O		5.090
4	C–C		4.261
5[b]	O–H (type *a*)		(I) 6.200
			(II) 6.700
	(type *b*)		6.400
	(intermol)		5.900

Table A1 *continued*

No.	Coordinates involved	Common atoms	Values[a]
6[b]	O···HO (type *a*)		(I) 0.150
			(II) 0.100
	(type *b*)		0.100
	(intermol)		0.200
7	C–H, C–H	C	−0.046
8	C–O, C–O	O	0.288
9	C–C, C–O	C	0.101
10	C–C, C–C	C	0.101
11	H–C–H (CCH_2O)		0.471
12	H–C–C (CCH_2O)		0.752
13	H–C–O (CCH_2O)		0.901
14	H–C–O (ring CH)		0.961
15	H–C–C (ring CH)		0.718
16	H–O–C		0.760
17	C–O–C		1.313
18	C–C–O		1.182
19	C–C–C		1.071
20	O–C–O		1.200
21	C–O, H–C–O	C–O	0.387
22	C–C, H–C–C	C–C	0.403
23	C–C(O), H–C–C	C	0.079
24	C–O, C–O–C	C–O	0.483
25	C–O, C–C–O	C–O	0.618
26	C–C, C–C–O	C–C	0.403
27	C–C, C–C–C	C–C	0.417
28	H–C–O, H–C–O	C–O	−0.005
29	H–C–C, H–C–C	C–C	0.105
30	H–C–O, H–C–C	H–C	0.115
31	H–C–C, H–C–C	H–C	0.012
32	H–C–C, H–C–C	C–C (*gauche*)	0.004
33	H–C–C, H–C–C	C–C (*trans*)	0.121
34	H–C–O, C–C–O	C–O	−0.031
35	H–C–C, C–C–C	C–C	−0.031
36	H–C–O, C–O–C	C–O (*gauche*)	0.004
37	H–C–C, C–C–O	C–C (*gauche*)	−0.113
38	H–C–C, C–C–C	C–C (*gauche*)	−0.052
39	H–C–C, C–C–C	C–C (*trans*)	0.049
40	C–C–O, C–C–O	C–O	−0.041
41	C–C–O, C–C–C	C–C	−0.041
42	C–O–C, O–C–C	C–O (*gauche*)	0.011
43	C–O–C, O–C–C	C–O (*trans*)	−0.011
44	O–C–C, C–C–O	C–C (*gauche*)	0.011
45	O–C–C, C–C–O	C–C (*trans*)	−0.011
46	C–C–C, C–C–O	C–C (*gauche*)	0.011
47	C–C–C, C–C–O	C–C (*trans*)	−0.011
48	C–C–C, C–C–C	C–C (*gauche*)	0.011
49	C–C–C, C–C–C	C–C (*trans*)	−0.011
50	C–O–C, O–C–O	C–O (*gauche*)	0.011
51	C–O–C, O–C–O	C–O (*trans*)	−0.011
52	torsion (C–O)		0.026
53	torsion (C–C)		0.024
54[b]	O···H–O (bending)		0.06
55[b]	H···O–C (bending)		0.06

[a] Units: mdyn/Å for stretching, mdyn Å/rad^2 for bending and torsion, and mdyn/rad for stretching–bending
[b] Force constants for hydrogen bonds. Refer to the text

APPENDIX 2

Table A2 Calculated wavenumbers and approximate description of the vibrational modes for cellulose crystal form I

Symmetry species				
A[a]		*B*		
$\theta = 0$[b]	$\theta = \pi$	$\theta = 0$	$\theta = \pi$	Modes[c]
3412	3412	3412	3412	ν(OH) (type *b*)
3372	3372	3372	3372	ν(OH) (type *a*)
3309	3309	3309	3309	ν(OH) (intermol)
3037	3037	3037	3037	ν(CH)
2972	2972	2972	2972	$\nu_{as}(CH_2)$
2953	2953	2954	2954	ν(CH)
2951	2950	2951	2950	ν(CH)
2940	2939	2939	2940	ν(CH)
2877	2877	2877	2877	$\nu_s(CH_2)$
1501	1501	1508	1510	δ(CH)
1475	1474	1474	1474	$\delta(CH_2) + \delta$(CH)
1467	1468	1467	1466	δ(CH)
1445	1446	1446	1445	$\delta(CH_2)$
1411	1410	1410	1411	δ(CH)
1398	1399	1406	1403	δ(OH) + δ(CH)
1391	1391	1390	1390	δ(OH) + δ(CH)
1367	1366	1370	1370	δ(CH)
1357	1357	1365	1365	δ(CH)
1354	1355	1350	1348	δ(CH)
1333	1337	1337	1336	δ(CH)
1292	1294	1303	1304	δ(CH)
1284	1283	1287	1288	δ(CH)
1263	1265	1273	1269	δ(CH) + w(CH_2)

Table A2 *continued*

Symmetry species				
A^a		B		
$\theta = 0^b$	$\theta = \pi$	$\theta = 0$	$\theta = \pi$	Modes[c]
1245	1245	1247	1248	t(CH_2)
1230	1234	1237	1235	δ(CH) + t(CH_2)
1187	1185	1191	1192	r(CH_2) + δ(CH)
1161	1159	1167	1163	δ(CH) + δ(skel)
1154	1155	1159	1160	ν(CC) + ν(CO) + δ(CH)
1138	1139	1143	1143	ν(CC) + ν(CO) + δ(CH)
1127	1126	1124	1124	δ(CH) + r(CH_2)
1116	1119	1111	1110	ν(CC) + ν(CO) + δ(skel)
1090	1089	1082	1082	δ(CH)
1069	1069	1075	1075	ν(CC) + ν(CO) + δ(CH)
1045	1045	1050	1051	ν(CC) + ν(CO) + δ(CH)
996	998	1028	1028	δ(CH) + r(CH_2)
980	980	983	984	δ(skel) + δ(CH)
965	965	970	973	ν(CC) + δ(skel) + δ(CH)
905	901	916	917	r(CH_2)
727	728			δ(skel) + δ(CH)
662	664	662	660	δ(skel) + δ(CH)
610	607	627	627	δ(skel) + δ(CH)
579	577	579	580	δ(skel) + δ(CH)
541	542	541	541	δ(skel)
		518	518	δ(skel) + δ(CH)
455	456	466	468	δ(skel)
452	450	447	445	δ(skel) + δ(CMO)
430	428	429	431	δ(MO · · · O) + τ(COH)
413	414	419	413	δ(skel) + δ(MO · · · H) + δ(COH) + ν(O · · · O:inter)
398	400	389	387	δ(skel)
348	349	382	377	δ(skel) + δ(MO)
		360	356	δ(skel) + δ(CH)
315	321	321	321	δ(skel) + δ(CH)
306	306	288	288	ν(OH · · · O:*a*,*b*) + δ(skel)
276	277	281	280	τ(CMOH) + ν(O · · · O:inter)
263	264	260	262	δ(skel) + ν(OH · · · O:*b*)
		227	226	ν(OH · · · O:*a*,*b*)
		211	202	ν(OH · · · O:*b*) + δ(skel)
194	193			δ(skel)
176	172			δ(skel) + τ(CMOH) + ν(OH · · · O:*b*)
150	150			δ(skel)
141	148	138	139	ν(OH · · · O:*b*) + δ(CMO)
		130	124	ν(OH · · · O:*b*) + δ(skel)
117	120			ν(OH · · · O:*a*,*b*)
105	110	111	107	δ(skel) + τ(skel) + ν(H · · · H:inter)
			105	τ(skel) + ν(OH · · · O:*b*)
95				τ(skel) + δ(skel) + δ(CO · · · H)
		84		τ(ether link)
			81	$L(T_b)$
80				$L(R)^+$
	77			$L(R)^- + \tau$(skel)
	54			$L(R)^-$
	41			$L(T_c)$
			34	$L(T_a)$

[a] Phase relation between the corner and centre chains in the unit cell

[b] Vibrational modes: ν, stretching; δ, bending; w, wagging; t, twisting; r, rocking; δ(skel), bending of skeletal ring; δ(CMO), bending of –C–CH_2–OH bond; δ(MO · · · H), bending of –CH_2– O · · · H hydrogen bond angle; τ(COH), torsion around C–OH bond; τ(CMOH), torsion around CCH_2–OH; τ(skel), torsion of skeletal ring; τ(ether link), torsion around the ether linkage between two rings; ν(OH · · · O), stretching mode of intramolecular hydrogen bond; L, lattice vibrational modes (refer to *Figure 6*)

APPENDIX 3

Three-dimensional elastic and compliance constants of poly(m-phenylene isophthalamide) crystal

The lattice dynamically calculated elastic (c) and compliance (s) tensors of PPIA crystal are as follows. The details of the calculation will be reported elsewhere[38].

$$c = \begin{bmatrix} 22.09 & 11.10 & 17.84 & -2.33 & -4.50 & 1.26 \\ & 40.87 & 17.63 & -1.57 & -3.03 & 4.62 \\ & & 137.37 & -3.17 & -9.02 & 3.05 \\ & \text{symmetric} & & 13.93 & 7.07 & -1.92 \\ & & & & 9.62 & -2.35 \\ & & & & & 6.05 \end{bmatrix} \text{GPa}$$

$$s = \begin{bmatrix} 5.99 & -1.36 & -0.47 & -0.36 & 2.41 & 0.85 \\ & 3.12 & -0.20 & -0.05 & -0.33 & -2.14 \\ & & 0.86 & -0.27 & 0.72 & 0.01 \\ & \text{symmetric} & & 11.61 & -8.85 & 0.50 \\ & & & & 19.62 & 4.20 \\ & & & & & 19.78 \end{bmatrix} \times 10^{-2}\ \text{GPa}^{-1}$$

The Young's modulus along the chain axis is calculated as 116.8 GPa.